Electronic Supplementary Material (ESI) for Journal of Materials Chemistry

Electronic Supplementary Information for the paper

Size and shape matter! A multiscale molecular simulation approach to polymer nanocomposites

by Radovan Toth, Francesca Santese, Simão P. Pereira, Daniel R. Nieto, Sabrina Pricl, Maurizio Fermeglia and Paola Posocco

Simulation procedure and computational details

The proposed computational procedure of the multiscale simulation and modeling is based on the following ansatz: 1) fully atomistic molecular dynamics simulations are perform to retrieve fundamental structural and energetical information at the molecular level; 2) the data gathered at point 1) are mapped into the corresponding structural and energetical information necessary to run coarse-grained simulations at a mesoscopic level; 3) the main output of point 2), i.e., the system mesoscopic morphologies and density distributions finally constitute the input for finite element calculations and macroscopic properties predictions. The core step in the entire computational recipe is undoubtedly constituted by point 2), or the mesoscale level simulations. In mesoscale modeling, the familiar atomistic description of the molecules is coarse-grained, leading to beads of material (representing the collective degree of freedom of many atoms). These beads interact through pair-potentials which capture the underlying interactions of the constituent atoms. The primary output of mesoscale modeling are phase morphologies with size up to the micron level. These morphologies are of interest *per se*, although little prediction of the material properties is available with the mesoscale tools. Finite element modeling then comes into play, and the material properties of interest can be calculated accordingly by mapping the material structures formed at the nanometer scale onto the finite element grid and coupling this information with the properties of the pure components that comprise the complex system. Using standard solvers the finite element code can then calculate the properties of the realistic structured material.

Atomistic molecular dynamics (MD) simulations

As mentioned above, atomistic MD simulations constitute the first MsM step, necessary to gather basic structural and energetical information of each PNC system at the molecular level. In particular, the interaction energies among all system components are of paramount importance, as they will, after proper remapping, constitute the major input parameter for performing mesoscale (MS) simulations. Hence, the choice of a reliable force field for the description of inter- and intra- molecular interactions in atomistic MD simulations is

a critical issue in the entire protocol. Our previous experience [1], coupled with a thorough literature survey [2,3], led us to the adoption of the *Compass* force field (FF) [4,5].

The optimized montmorillonite (MMT) model was taken from our previous work [1(c,k)]. Starting from the crystal coordinates of Mg/Al hydrotalcite as determined by Bellotto et al [6], the model of hydrotalcite (HT) was built and optimized by adapting the procedure adopted for MMT [1(c,k)]. The unit cells of sepiolite (SEP), boehmite (BOE), and titanium dioxide (rutile form, TiO_2) were optimized starting from the original structures available in the *Materials Studio* (v.5.5, Accelrys, USA) structure database. Table 1 lists the main structural parameters for all nanoparticles considered. To generate a mineral surface apt for simulation, the lattice constant *c* of each mineral cell was extended to 150 Å [1(c,d)], while the lateral dimensions of the cell were increased to the point where the total number of atoms in each model was approximately equal.

Table 1.

Main structural parameters for the optimized molecular models of the nanoparticles considered in this work.

Model	Lattice geometry	Space group	Lattice parameters					
			a (Å)	*b* (Å)	*c* (Å)	α (Å)	β (Å)	γ (Å)
MMT	MON[a]	*C2/m*	5.20	9.20	10.1	90	99	90
HT	HEX[b]	*R3m*	3.05	3.05	22.8	90	90	120
SEP	ORT[c]	*Pnan*	13.4	26.8	5.28	90	90	90
BOE	ORT[c]	*A/mnm*	2.85	12.2	3.69	90	90	90
TiO_2	TET[d]	*P4/mnm*	4.59	4.59	2.95	90	90	90

[a]MON = monoclinic. [b]HEX = hexagonal. [c]ORT = orthorhombic. [d]TET = tetragonal.

The model structures of the MMT and HT surface modifiers (i.e., quaternary ammonium salts and C_{16}-C_{18} fatty acids, respectively) were built and subjected to an initial energy minimization using *Compass* [4,5], the convergence criterion being set to 10^{-4} kcal/(mol Å). A thorough conformational search for these molecules was then performed using a well-validated Molecular Mechanics/Molecular Dynamics simulated annealing (MDSA) protocol [7].

The generation of accurate model amorphous structures for polymers was conducted as follows. First, the constitutive repeating unit (CRU) of each polymer was built and its geometry optimized by energy minimization again using *Compass* [4,5]. Hence, each CRU was polymerized to a conventional degree of polymerization (DP) equal to 53 for PP, 25 for Nylon and 12 for TPU. Polymers of similar lengths have been already successfully employed by us in similar studies [1(c,d)]. Explicit hydrogens were used in all model systems. The Rotational Isomeric State (RIS) algorithm [8] as modified by Theodorou and Suter [9] was used to

create the initial polymer conformation at T = 298 K. Each resulting polymer structure was then extensively relaxed to minimize energy and avoid atom overlaps. Subsequently, an NVT MD with temperature increasing to 373 K during 200 ps followed by an NVT MD at 373 K for 500 ps, and a cooling to 298 K over 200 ps was performed on each polymer sample.

After each component was modeled, the overall PNC systems were built following our previous works [1(c,d)]. Then, molecular dynamics (MD) simulations in the canonical (NVT) ensemble were run at T = 298 K. Each MD run consisted of an equilibration phase of 50 ps, followed by a data collection phase extended up to 0.5 ns. The Berendsen thermostat was used to control temperature, while an atom-based cutoff and the Ewald summation technique [10] were employed to treat dispersion and electrostatic nonbonded interactions, respectively. From the equilibrated part of the MD trajectory of each PNC, the interactions energies among all system components were extracted according to the procedure described in detail in [1(c,d,i)]. Briefly, the total potential energy of ternary PNC system (e.g., PP, HT and the C_{16}-C_{18} fatty acids (FA) clay surface modifiers) can be written as:

$$E_{(PNC)} = E_{PP} + E_{HT} + E_{FA} + E_{PP/HT} + E_{PP/FA} + E_{HT/FA} \quad (1)$$

where the first three terms represent the energy of PP, HT, and FA (consisting of both valence and nonbonded energy terms), and the last three terms are the interaction energies between each of two component pairs (made up of nonbonded terms only). By definition, the binding energy between each pair of PCN components (E_{bind}) is the negative of the corresponding interaction energy. Thus, to estimate the binding energy between, say, the polymer and the clay ($E_{bind(PP/HT)}$), starting from an equilibrated snapshot of the corresponding MD trajectory a subsystem is created by deleting the FA molecules, and the corresponding $E_{PP/HT}$ is evaluated. Next, the HT platelets are deleted from the MD frame, yielding E_{HT}. Lastly, from the binary system, the PP chains are in turn deleted, leading to the value of E_{PP}. Then, by definition:

$$E_{bind(PP/HT)} = E_{PP} + E_{HT} - E_{PP/HT} \quad (2)$$

Similarly, the binding energies $E_{bind(PP/FA)}$ and $E_{bind(HT/FA)}$ can be estimated as:

$$E_{bind(PP/FA)} = E_{PP} + E_{FA} - E_{PP/FA} \quad (3)$$

$$E_{bind(HT/FA)} = E_{HT} + E_{FA} - E_{HT/FA} \quad (4)$$

In the case of modified nanoparticles (i.e., MMT and HT), starting from an equilibrated NVT MD snapshot further MD simulations in the isothermal-isobaric (NPT) ensemble were performed to estimate the interlayer (basal) spacing d among the mineral layers [1(c,k,i)]. In this case, during each MD both mineral layers were

treated as rigid bodies by fixing all cell dimensions except for *c*, and all atoms in the interlayer space (including ions and counterions) were allow to move without any constraint.

Figure 1 presents a selected example of the atomistic models employed in the MD simulations for the calculation of the interaction energies (NVT MD) and, specifically for layered nanoinclusions, the estimation of the interlayer *d* spacing (NPT MD), respectively.

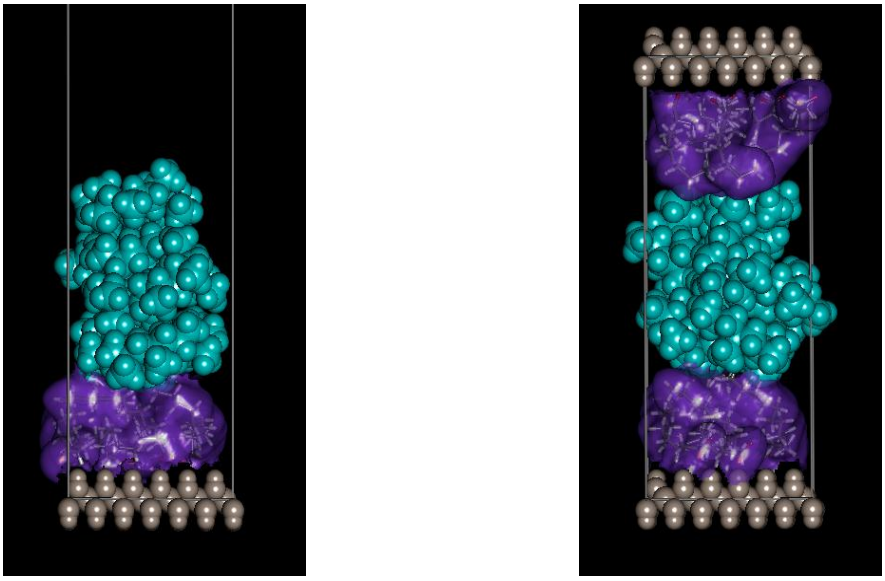

Fig. 1. (Left) Equilibrated molecular model system used in atomistic NVT MD simulations for binding energy calculations in PNC systems with surface modifier. (Right) Equilibrated molecular model systems used in atomistic NPT MD simulations for interlayer spacing determination in PNC with surface modifier. The system PP/HT/FA is shown as an example.

Mesoscale simulations of PNCs

In order to simulate the morphology of the nanocomposite systems at a mesoscopic level, we used the Dissipative Particle Dynamics (DPD) [11,12] simulation tool as implemented in the *Materials Studio* (v. 5.5) DPD modeling suite. In DPD, a group of atoms is coarse-grained into a bead, thereby substantially reducing the number of particles to be simulated. Further, rather than interact through Lennard-Jones forces, each bead feels a simple soft pair-wise conservative potential which embodies the essential chemistry of the system. This force is of short range, and has a simple analytical form, which results in fast computation per time step and, hence, provides the opportunity to expand the simulation from nanoseconds to real time periods. Figure 2 shows, as an example, a comparison between the atomistic (MD) and coarse-grained (DPD) model for one of the clay surface modifiers studied in the present work.

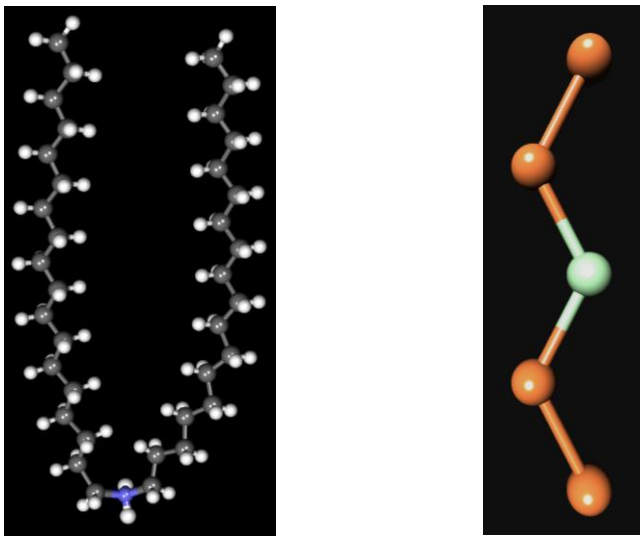

Fig. 2. Atomistic (MD, left) and coarse-grained (DPD, right) representation of surface modifier $(H_3C)_2N(C_{18}H_{37})_2$ of Cloisite 15A and 20A. In the atomistic view, the quaternary ammonium salt is portrayed as atom-colored sticks-and-balls (atom color code: N, blue; C, gray; H, white). The coarse-grained DPD beads are colored according to the corresponding bead type (T, orange; light green, H).

Similar to molecular dynamics, the time evolution of each DPD particle can be calculated by solving Newton's second law:

$$\frac{d\boldsymbol{r_i}}{dt} = \boldsymbol{v}_i \qquad \frac{d\boldsymbol{p}_i}{dt} = \sum_{i \neq j} \boldsymbol{F}_{ij} \tag{5}$$

where $\boldsymbol{r}_i$, $\boldsymbol{v}_i$, and $\boldsymbol{p}_i = m\boldsymbol{v}_i$ are the position, velocity and momentum vectors of particle i, respectively, and $\boldsymbol{F}_{ij}$ is the total inter-particle force exerted on particle i by particle j. $\boldsymbol{F}_{ij}$ is, in turn, the sum of three contributions. Each contribution has a parameter that sets the relative magnitude of the interactions and a functional form that determined how the forces varies with increasing separation of the beads up to a critical distance r_c, where these forces vanish. The first type of force contributing to $\boldsymbol{F}_{ij}$ is a conservative interaction that corresponds in purpose, although not in its functional form, to the Lennard-Jones interactions between two atoms in an MD simulation. It allows beads to be given an identity, so that chemically different beads feel mutual attraction or repulsion. The magnitude of this conservative force is related to the compressibility of the system being simulated, and is given by:

$$\boldsymbol{F}_{ij}^{C} = a_{ij}\frac{1-r_{ij}}{r_c}\boldsymbol{r}_{ij} \tag{6}$$

for $r_{ij} < r_c$ and zero otherwise. The range of $\boldsymbol{F}_{ij}^{C}$ is set by r_c, and a_{ij} is the maximum force between beads of type i and j. r_{ij} is the distance between the centers of beads i and j, and $\boldsymbol{r}_{ij}$ is the unit vector pointing from bead j to

bead *i*.

The other two forces that the DPD bead experience are a dissipative and a random force that together constitute a thermostat that extract energy to the system and adds energy to the system, respectively. Importantly, unlike the thermostats commonly employed in MD simulations, the DPD thermostats conserves momentum locally, and it is this that allows the hydrodynamic interactions in the systems to propagate.

Lastly, molecules in DPD are built by tying beads together using Hookean springs with the potential given by:

$$U_{bb}(i, i+1) = \frac{1}{2} k_{bb} (r_{ii+1} - l_0)^2 \quad (7)$$

where *i,i+1* label adjacent beads in the molecule. The spring constant, k_{bb}, and the unstretched length l_0, are chosen so as to fix the average bond length to a desired value. Chain stiffness is modeled by a three body potential acting between adjacent bead triples in a row:

$$U_{bbb}(i-1, i, i+1) = k_{bbb}(1 - cos(\phi - \phi_0)) \quad (8)$$

in which the angle ϕ is defined by the scalar product of the two bonds connecting the pair of adjacent beads *i*-1, *i*, and *i*+1, and ϕ_0 is the corresponding equilibrium value.

In the framework of our multiscale approach to PNCs simulation, the interaction parameters needed as input for the mesoscale level DPD calculations have been obtained by a mapping procedure of the binding energy values between different species obtained from simulations at a lower (atomistic) scale [1(e,i)]. The complex procedure for mesoscale simulation of our PNC systems consists of several steps: i) choice the bead size, ii) determination of system dimension and bead numbers, and iii) definition of bead-bead interaction parameters [16(e,i,l-n)]. In the case of surface-modified nanocomposites, according to the fundamental DPD concept that different DPD bead types should have equal roughly volumes, and starting with the surface modifier molecules (which consist of a strongly polar head and one/two almost apolar tails) we considered them as made up by two different type of beads *H* and *T*, respectively. The chosen bead volume had an average value of 130 Å^3, roughly corresponding to that of a single PA6 monomer, (134 Å^3), 2 PP monomers (60 Å^3/monomer), and 0.5 TPU monomer (272 Å^3/monomer), respectively. The corresponding mesoscopic polymer chains were chosen to be constituted of 100 beads of type *P*. Having determined the bead size, and fixed the DPD system density ρ = 3, [12(b)] the corresponding characteristic dimension of the mesoscopic system (i.e. the cutoff distance r_c) was obtained via the simple relationship:

$$r_c = (\rho V_b)^{1/3} \quad (9)$$

where V_b is the volume of a bead, yielding r_c = 7.4 Å. As mentioned above, this value represents the soft potential cutoff distance; importantly, however, it also corresponds to the length of one of the unit cells in the DPD simulation box.

Taking again the PP/HT/FA PNC as a proof-of-concept, the corresponding DPD system was chosen to be constituted by 20 × 20 × 6 unit cells; accordingly, the simulation cell was characterized by effective dimensions of 14.6 nm × 14.6 nm × 4.4 nm. To represent the filler surface, a repulsive wall in the simulation box perpendicular to the *z*-axis at the origin was employed. Further, we introduced a bead type *M* with no connectivity and no repulsion towards the wall, in order to fill the space between the two wall surfaces, thus representing a nanofiller layer.

Having set the DPD box dimensions, we next calculated the number of clay modifiers that had to be used at the mesoscopic levels in order to match the model architecture employed in the corresponding MD simulations. In the case of HT, since the surface of the atomistic molecular model employed has an area of approximately 278.2 Å^2 (i.e., 18.3 Å × 15.2 Å), with a total surface charge of 4e, 4 fatty acid molecules were placed on it to neutralize the system. On the other hand, the surface in the corresponding DPD model had an area of roughly 21351 Å^2 (i.e., 146.1 Å × 146.1 Å), and bears a charge of 308e. Accordingly, the total number of FA molecules to be inserted in the DPD box is 616 (308 for each layer). The number of HT beads to be inserted can in turn be calculated once the volume of the HT platelet molecular model (1196 Å^3) is known. This leads to a total of 1417 HT beads. Finally, being 7200 the total number of beads in the box, and the number of FA beads estimated to be 1848 (= 616 × 3), the number of polymer beads to use to fill the interlayer spacing is 3935 (= 7200 – (1848 + 1417). A parallel approach and utterly similar concepts were used to build all remaining PNCs. In this cases, however, the corresponding mesoscopic cells contained only two type of beads; indeed, beads of the type *M* were again used to represent the filler (i.e., SEP, BOE, and TiO_2), and beads of the type *P* were still employed for the polymers. The DPD cell dimensions were such that enough space was available between the filler surfaces, in keeping with the fact that these systems were all well-dispersed/exfoliated. The main characteristics of all DPD PNC systems studied, together with the mesoscopic architecture of the surface modifiers (when present) are given in Table 2.

The next, important issue in DPD simulations is to capture the essential intra-and intermolecular interactions taking place among all molecular actors of the mesoscopic simulations as expressed by the values of the conservative parameter a_{ij}. This quantity accounts for the underlying chemistry of the system considered. In this work, we employed a well-validated strategy that correlates the interaction energies

estimated from a lower scale (atomistic MD) simulations to the mesoscale a_{ij} parameter values [13]. Following this computational recipe, the interaction energies among all PNC system components estimated using Eqs. (1)-(4) were rescaled onto the corresponding mesoscale segments adapting the procedure described in detail in [1(e,i)]. The bead-bead interaction parameter for the polymer beads *P* was set equal to a_{PP} = 25, in agreement with the value of DPD density ρ = 3 [12(b)]. The value of the polymer-filler interaction (i.e., a_{PM}) was chosen to reflect the corresponding atomistic energy value [1]. Once these two parameters were assigned, all the remaining bead-bead interaction parameters required for the DPD simulations were easily obtained, starting from the relevant atomistic interaction energies values.

Table 2.

Main characteristics of all DPD PNC systems studied in this work.

System	Number of bead types				Total number of beads	Cell dimension	Surfactant bead structure
	M	*H*	*T*	*P*			
PP/C10A	1622	204	408	3766	6000	20x20x5	1H-2T
PP/C15A	1622	268	1072	5438	8400	20x20x7	2T-1H-2T
PP/C20A	1622	204	816	4588	7200	20x20x6	2T-1H-2T
PP/C30B	1622	204	408	3766	6000	20x20x5	1H-2T
PP/ODA	1622	204	408	3766	6000	20x20x5	1H-2T
PA6/C20A	1622	204	816	4588	7200	20x20x6	2T-1H-2T
PA6/C30B	1622	204	408	4966	7200	20x20x6	1H-2T
PA6/M3C18	1622	204	408	3766	6000	20x20x5	1H-2T
TPU[a]/C30B	1622	204	408	4966	7200	20x20x6	1H-2T
PP/HT/FA	1417	616	1232	3935	7200	20x20x6	1H-2T
PP/SEP	1946	-	-	12454	14400	20x20x12	-
PP/BOE	1558	-	-	12842	14400	20x20x12	-
PP/TiO_2	940	-	-	13460	14400	20x20x12	-

As anticipated above, we made use of the option available in the DPD commercial software of including a smooth wall in the simulation box during the construction of the mesoscopic model of the nanofillers. A solid flat wall in DPD is usually built as an ensemble of locally freezing DPD particles [14,15]. The frozen particles behave as normal fluid particles but maintain a fixed position and velocity. Therefore, the wall interacts with each bead in the system with a potential of the same form as the bead-bead conservative force. Thus, as all

beads/wall repulsive parameters are concerned, we decided to simply scale up the interaction parameters with the nanofiller beads *M* by a factor of 10 [1(e,i,k)]. In this way, we preserved the proportion of the interaction energies between clay and organic species and, at the same time, we prevented the beads from crossing the wall, taking an effective flat solid surface.

Finite elements (FEM) calculations

The last step of the proposed MsM procedure is constituted by the prediction of a set of important macroscopic properties for the considered polymer nanocomposites as a function of filler loading. To this purpose, finite element (FE) calculations were performed using the software *Palmyra* (v. 2.5, MatSim, Zürich, CH). This software has been validated on different composite material morphologies by several authors, including us [1(i,k,l),16,17], yielding reliable results. FE calculations were applied in order to analyze both platelet stacks and overall nanocomposite properties, using fixed (*Mesoprop* technique) and variable grid, respectively. In particular, the Young modulus *E*, the thermal conductivity κ, and the gas permeability *P* were the macroscopic properties of election, since not only these quantities are of primary industrial interest but, perhaps more importantly, direct comparison with the corresponding experimental data could be made [18].

MesoProp technique [19] is a method based on finite elements for estimating properties of a complex material starting from the density distribution at mesoscale. The method used the results of a mesoscale simulation under the form of three dimensional density maps and transforms such information into a fixed grid that is used for the integration of the equations for determining macroscopical properties. *MesoProp* [19] uses a numerical method to determine the overall properties of composites, with arbitrary morphologies from the properties of the components based on small homogeneous grid elements. The morphology is defined by a number of phases in a periodically continued base cell of cubic or orthorhombic shape, where the phases may consist of any material. Accordingly, the resolution depends solely on the number of grid elements used.

The FE calculations of the macroscopic properties consisted of these steps: 1) definition of an appropriate reactive volume element (RVE), representative of the different morphologies characterizing such complex materials as polymer nanocomposites, 2) definition of the degree of filler exfoliation/dispersion, and 3) generation of apt surface and volume meshes in order to calculate the final macroscopic property by numerical approach. Following our previous work [1(i, k)], MMT and HT particles (both single particles and stacks) were modeled as disks with a toroidal rim. Each platelet thickness was defined by the height of the corresponding symmetry axis *h* and diameter *D*, thus being characterized by an aspect ratio of $\alpha = D/h$. By

setting D = 120 nm and h = 1 nm for each single particle, the aspect ratio a was equal to 120, a value in agreement with common literature data for layer silicates.

Orientation to the platelets was imparted by assigning a value of 0.06 to the eigenvalues 1 and 2. Accordingly a value of 0.88 was automatically assigned to the eigenvalue 3. A highly exfoliated system was defined as having 32 platelets with an aspect ratio of 120 and 8 stacks of two platelets each. Such a system corresponds to 66.7% exfoliated platelets. The aspect ratio of the stacks ranged from 10 to 13, according to the different basal spacing obtained from the corresponding MD simulations. To simulate a weight fraction Φ_w of 4.6% w/w for all MMT and HT PNCs, a volume fraction Φ_v of 1.5% v/v was used in the case of PP-based PNCs, while a value of Φ_v = 1.9% v/v was employed for TPU- and PA6-based systems, respectively.

TiO_2 particles were considered as spheres with diameter φ_{TiO_2} = 20 nm. A volume fraction of 1.07% v/v was used, resulting in a corresponding weight fraction of 4.6% w/w. Boehmite is generally synthesized in crystallites of a platelet or rod shape. The widely employed commercial sample Disperal, however, consists of small crystallites agglomerated. During processing, the agglomerates decrease in size, but still the complete dispersion of the crystallites cannot be achieved [20]. Accordingly, this system was defined considering spherical agglomerates of BOE with an average φ of 140 nm [21]. A volume fraction of 1.43% v/v was used, corresponding to a system with a weight fraction of 4.6% w/w.

Finally, the commercial CD1 sepiolite fibers were assumed to have a length L = 200 nm and a diameter φ_{SEP} = 10 nm. A Φ_v = 2.1% v/v was considered, corresponding to a system with Φ_w = 4.6% w/w.

Table 3 summarized the FEM details adopted in this work.

Interfacial interactions, however, invariably develop in composite systems based on untreated nanofillers, due to the ever-existing van der Waals or electrostatic forces among the particles and the polymer chains. These lead to the formation of a non-negligible interface which, in turn, may considerably influence the macroscopic properties of the relevant PNC. To account for the presence of this interphase layer in the BOE, SEP, and TiO_2 systems, as determined from mesoscale simulations, we resorted to a *pseudo* "core-shell" model particles at the FEM level. These models consist in spherical (for BOE and TiO_2) and spherocylindrical (for SEP) particles with radius equal to the sum of the pristine nanoparticle radius (constituting the "core" part of the particle) and the interface thickness (making up the "shell"). The overall, main thermophysical properties of these particles were then estimated by mediating each corresponding property of the nanoparticle core (i.e., the pure nanoparticle property) and of the interphase (as obtained by running fixed-grid calculations using the mesoscopic density distribution as input information) by the corresponding volumetric fractions.

Table 3.

Main characteristics of the different FEM PNC models.

System	Filler model	*D* (nm)	*L* (nm)	# nodes	# tetrahedra	Mesh quality
PA6/MMT/quat	SP[a]	1	120	4-6x10^5, 1.2x10^6*	3-4x10^6, 7x10^6*	0.25-0.3
PP/MMT/quat	SP[a]	1	120	4-6x10^5, 1.2x10^6*	3-4x10^6, 7x10^6*	0.25-0.3
TPU/MMT/quat	SP[a]	1	120	4-6x10^5, 1.2x10^6*	3-4x10^6, 7x10^6*	0.25-0.3
PP/HT/FA	SP[a]	1	120	4-6x10^5, 1.2x10^6*	3-4x10^6, 7x10^6*	0.25-0.3
PP/SEP	SC[b]	12.4[d]	200	3x10^5	2.7x10^6	0.27
PP/BOE	SPH[c]	142.2[d]	-	2x10^4	2x10^5	0.4
PP/TiO_2	SPH[c]	23.4[d]	-	3x10^5	2x10^6	0.3

[a]SP = Single platelets. [b]SC = Spherocylinders. [c]SPH = Spheres. [d]The reported *D* values were obtained by summing the value of the pristine nanoparticles and the interface layer thickness, as estimated from the corresponding mesoscopic density maps. *This value was used in the case of thermal conductivity and gas permeability.

As mentioned previously, the density profiles of each component obtained from mesoscale simulations were used as an input for macroscopic property calculation of the stacks for intercalated systems according to the MsM procedure.

Finally, the bulk properties of each pure component of the diverse PNCs listed in Table 6 constituted the last information necessary to run FEM calculations. All listed data were obtained from literature [22]. Thermal conductivities of MMT, BOE, SEP and HT were assumed to be the same and equal to the value found for bentonite clay [1(i)]. As each nanofiller itself was considered to be impermeable to gases, a very low permeability value (i.e., P = 0.0001 barrer) was selected.

It is worth noticing here that high-quality mesh generation is of fundamental importance in order to calculate realistic values of the macroscopic properties of the nanocomposite materials. Since a thorough discussion on this topic is beyond the main scope of the present paper, the interested reader is referred to another paper from our group dealing with this issue in detail [1(k)].

References

[1] a) Fermeglia M, Ferrone M, Pricl S. Fluid Phase Equilib 2003; 212: 315–29; b) Fermeglia M, Ferrone M, Pricl S. Mol Simul 2004; 30: 289–300; c) Toth R, Coslanich A, Ferrone M, Fermeglia M, Pricl S, Miertus S, Chiellini E. Polymer 2004; 45: 8075–83; d) Toth R, Ferrone M, Miertus S, Chiellini E, Fermeglia M, Pricl S. Biomacromolecules 2006; 7: 1714-19; e) Scocchi G, Posocco P, Fermeglia M, Pricl S. J Phys Chem B 2007; 111: 2143–51; f) Cosoli P, Scocchi G, Pricl S, Fermeglia M. Microporous Mesoporous Mater 2008; 107: 169-79; g) Fermeglia M, Pricl S. Prog Org Coat 2007; 5: 187–99; h) Fermeglia M, Cosoli P, Ferrone M, Piccarolo S, Mensitieri G, Pricl S. Polymer 2006; 47: 5979–89; i) Toth R, Voorn DJ, Handgraaf JW, Fraaije JGEM, Fermeglia M, Pricl S, Posocco P. Macromolecules 2009; 42: 8260-70; j) Scocchi G, Posocco P, Danani A, Pricl S, Fermeglia M. Fluid Phase Equilibria 2007; 261: 366–74; k) S.P. Pereira, G. Scocch, R. Toth, P. Posocco, D.R. Nieto, F. Santese, S. Pricl and M. Fermeglia, J. Colloid Interface Sci. 2011, submitted; l) Scocchi G, Posocco P, Handgraaf JW, Fraaije JGEM, Fermeglia M, Pricl S. Chemistry - A European Journal 2009; 15: 7586-92; m) Posocco P, Posel Z, Fermeglia M, Lísal M, Pricl S. Chem J Mater Chem 2010; 20: 10511-20; n) Maly M, Posocco P, Pricl S, Fermeglia M. Industrial & Engineering Chemistry Research 2008; 47: 5023-38.

[2] Minisini B, Tsobnang F. Composites Part A: Applied Science and Manufacturing 2005; 36: 539-44.

[3] a) Zhang H, Lu X, Leng Y , Fang L, Qu S, Feng B, Wang JWJ. Acta Biomaterialia 2009; 5: 1169–81; b) Sutton S, Sposito G. Geochimica et Cosmochimica Acta 2006; 70: 3566–81; c) Han Y, Elliott J. Computational Materials Science 2007; 39: 315–23.

[4] Sun H. J Phys Chem B 1998; 102: 7338-64.

[5] Rigby D. Fluid Phase Equilib 2004; 217: 77-87.

[6] Bellotto M, Rebours B, Clause O, Lynch J. J Phys Chem 1996; 100: 8527-34.

[7] Fermeglia M, Pricl S. AIChE J 1999; 45: 2619-27.

[8] Flory PJ. Principles of Polymer Chemistry. Ithaca, NY: Cornell University Press; 1974.

[9] Theodorou DN, Suter UW. Macromolecules 1986; 19: 139-54.

[10] Ewald PP. Ann Phys 1921; 64: 253-87.

[11] Hoogerbruge PJ, Koelman JMVA. Europhys Lett 1992; 18: 155-60.

[12] a) Koelman JMVA, Hoogerbruge PJ. Europhys Lett 1993; 21: 363-8; b) Groot RD, Warren PB. J Chem Phys 1997; 107: 4423-35.

[13] a) Posocco P, Fermeglia M, Pricl S. J Mater Chem 2010; 20: 7742-53; b) Posocco P, Pricl S, Jones S, Barnard A, Smith DK. Chem Sci 2010; 1: 393–404; c) Jones SP, Gabrielson NP, Wong CH, Chow HF, Pack DW, Posocco P, Fermeglia M, Pricl S, Smith DK. Mol. Pharmaceutics 2011; 8: 416–29.

[14] Maiti A, McGrother SJ. Chem Phys 2004; 120: 1594-601.

[15] Revenga M, Zuniga K, Espanol P, Pagonabarraga I. Int J Mod Phys C 1998; 9: 1319-31.

[16] Osman MA, Mittal V, Lusti HR. Macromol Rapid Commun 2004; 25: 1145-9.

[17] Heggli M, Etter T, Wyss P, Uggowitzer PJ, Gusev AA. Adv Eng Mater 2005; 7: 225-9.

[18] Tabuani D, Ceccia S, Camino G. Macromol Symp 2011; 301: 114-27.

[19] Gusev AA. J Mech Phys Solids 1997; 45: 1449-59.

[20] Streller RC, Thomann R, Torno O, Mulhaupt R. Macromolecular Materials and Engineering 2008; 293: 218-27.

[21] 6th EC FP IP *MultiHybrids* (026685-2IP) project consortium, private communication.

[22] PP data sheet: https://polymers.lyondellbasell.com/; b) Crawford RJ. Plastics Engineering (3rd Edition). Elsevier; 1998; c) Plastic materials data base (IDES): http://www.ides.com; d) Massey, L.K. Permeability Properties of Plastics and Elastomers - A Guide to Packaging and Barrier Materials (2nd Edition). William Andrew Publishing/Plastics Design Library; 2003; e) PA6 data sheet: http://www.rhodia.com; f) Ho WK, Koo JH, Ezekoye OA. Journal of Nanomaterials 2010; 2010: 1-11; g) TPU data sheet: htttp://www.basf.com; h) Fornes TD, Paul DR. Polymer 2003; 44: 4993-5013; i) Almanza R, Lozano MC. Solar Energy 1990; 45: 241-5; j) Winkler J. Titanium Dioxide. European Coating Literature; 2003 ; k) http://www.ceram.com; l) Bilotti E, Zhang R, Deng H, Quero F, Fischer HR, Peijs T. Composites Science and Technology 2009; 69: 2587-95; m) Gallas MR, Piermarini GJ. Journal of the American Ceramic Society 1994, 77: 2917-20, n) Thyveetil MA, Coveney PV, Suter JL, Greenwell HC. Chemistry of Materials 2007; 19:5510-23.